RESEARCH PAPER

Effectiveness of MWCNTs and GO Polymeric Nanocomposites with PANA-Epoxy in Inhibiting Corrosion of Low Carbon Steels

Wasan Abdulfatah Hussen *, *Ahmed Najem Abd, Abdulwahhab H. Majeed*

Department of Chemistry, College of Science, University of Diyala, Diyala, Iraq

ARTICLE INFO

ABSTRACT

The present study involved the synthesis of graphene oxide and polyanthranilic acid, along with the oxidation of multi-walled carbon nanotubes, to produce MWCNTs-COOH. The polyanthranilic acid solution was mixed with epoxy resin to prepare the mother solution. Then the polymeric nanocomposites (GO/Epoxy-PANA, MWCNTs/Epoxy-PANA) were prepared. The prepared materials were characterized by XRD, EDX and SEM. Finally, polymeric coatings were prepared, which consist of adding the mother solution and hardener with graphene oxide and oxidized carbon nanotubes, which are corrosion resistant. It was also found that the inhibition efficiency increased in the case of MWCNTs / Epoxy-PANA more than GO / Epoxy-PANA. On the other hand, the coating samples were examined by (SEM) and the results were recorded. The effects on activation energy (Ea), enthalpy (ΔH) and entropy (ΔS) were also studied.

How to cite this article

INTRODUCTION

In numerous fields, corrosion poses a significant and potentially hazardous challenge. Presently, several scholars concentrate on the utilization of nanocomposite coatings as an efficacious approach to forestall steel corrosion. The current overview investigates the potential implementation of nanocomposite coatings for corrosion management. Recent studies on corrosion inhibition are scrutinized herein. Diverse factors, such as the nature of nanomaterials, their sizes, concentrations, blending, and additives, impact the effectiveness of nanocomposite coatings [1]. Nanocomposites have gained great popularity in their use for this purpose, due to the attractive structures they produce when mixed, and their ability to impede corrosion by forming a distinct layer between the corrosive solution and the target metal (specifically, low carbon steel). The importance of nanocomposite anti-corrosion coatings in a variety of fields. Many polymeric nanocomposites have been widely used in this field, such as (MWCNTs), which include nanotubes, for example (carbon nanosheets and sheets), graphene oxide and its derivatives, and various types of polymers, including (epoxy polymers).(polyaniline, and polymers), its derivatives (polyurethane) and for example (polyurethane) (polyanthranilic acid) . Materials, whether made or naturally produced, have the ability to exhibit essential properties of the starting material, including high strength, stiffness, and high modulus. The process of separating chemically distinct phases through a

* *Corresponding Author Email: scichemms2202@uodiyala.edu.iq*

specific interface is known as thermal expansion [2]. Polymeric components of composite materials comprise two fundamental constituents, namely the matrix phase and the dispersed phase. The former, which is a continuous component of the body (dispersion phase), encompasses the composite and imparts it with a volumetric shape and can be constituted of polymeric, metallic or ceramic materials. The latter, on the other hand, is the structural component (dispersed phase) that defines the internal structure of the composite and imparts it with a solid shape. Dispersed phases can assume the form of fibers, particles, flakes or whiskers [3]. Polymeric Nanotechnology represents the manipulation of matter at the atomic, molecular, or supra-molecular scale within the size range of 1 nm to 100 nm in at least one dimension of its shape. Nanochemistry involves the study of interactions amongst atoms or molecular materials ranging in size from 1 nm to 100 nm [4]. Therefore, the adsorption of positively charged corrosion inhibitors is advantageous. The ligands consist of atoms that coordinate with the ions of the oxidized complexes, and their unpaired electrons occupy the empty orbitals of the said ions. Thus, the coordination bond formed becomes positively charged, which leads to the conversion of the bonding molecule into a positively charged corrosion inhibitor [5-14]. In the synthesis of metal-organic, organic ligands, such as (MWCNTs /Epoxy-PANA, GO /Epoxy-PANA), are favored among the polymeric varieties, since they comprise heteroatoms, including O. These heteroatoms exhibit the capability to establish coordinate bonds with metal atoms located on the surface of low carbon steel, thereby facilitating their adsorption onto the said surface. Consequently, these heteroatoms often serve as active adsorption sites for organic matter materials, thereby playing a crucial role in corrosion inhibition. Addition, the high porosity of the organic material enables the active sites to be fully exposed, facilitating their effective adsorption onto the surface of carbon steel, thus achieving the ultimate goal of corrosion protection. Simultaneously, the polymeric materials play an essential role in this process.[15–17].

Fields.Among these polymeric materials, graphene oxide-polymer and carbon nanotube-oxidized polymer nanocomposites have garnered considerable attention due to their unique blend of characteristics arising from graphene oxide and carbon nanotube-oxidized polymers. The corrosion of nanocomposite metal structures poses a significant challenge to virtually all industries.Graphene oxide-polymer nanocomposites have gained significant attention in recent years due to their unique combination of properties derived from graphene oxide and polymers. These nanocomposites metals structures' corrosion poses a major hurdle to almost all industries. Given the multifarious objectives of augmenting corrosion resistance, minimizing financial expenditures, and enhancing occupational safety, guaranteeing the durability of these structures is of paramount importance. Organic coatings are regularly employed to shield metallic structures from corrosion. It is generally believed that these polymeric coatings function as a physical barricade between the metal substrate and the corrosive environment[18-21]. Graphene oxide, a 2D material consisting of graphene sheets functionalized with oxygen groups, has exceptional mechanical, thermal, and electrical properties. Despite this, solvent-based epoxy coatings are typically used in highly aggressive environments due to their superior adhesion to metals, chemical resistance, processability, and cost-effectiveness. However, the hydrophilic hydroxyl groups in epoxy coatings make them susceptible to hydrolytic degradation in humid conditions and the exposure to corrosive electrolytes may initiate and propagate cracks in the coating. As a result, agents such as water, oxygen, Cl−, and H+ can penetrate through the coating defects and access the metal/coating interface, leading to reduced coating adhesion and an increase in metallic substrate corrosion [22-24]. Coatings are widely used as commercial coatings in highly demanding applications. To surmount this challenge, scholars have concentrated on integrating graphene oxide and carbon nanotube-oxidized into polymers, such as polyaniline (PANI), or one of its derivatives, such as poly (o-phenylene diamine), poly (p-phenylene diamine), poly (anthranilic acid), Poly (o-toluidine), and Poly(m-toluidine), among others, to produce polymer nanocomposites [25-29]. Poly Anthranilic Acid (PANA) is an electrically conducting polymer that is recognized for its high electrical conductivity, environmental stability, and processability. It can be synthesized via the oxidative polymerization of anthranilic acid [30]. PANA offers a conductive pathway within the nanocomposite, facilitating charge transfer and increase resistance corrosion.

The incorporation of PANA enhances corrosion inhibition of the nanocomposite, leading to reduce of corrosive and improved charge storage and energy dissipation capabilities[30-32]. Graphene oxide (GO) oxide and carbon nanotube-oxidized (MWCNTs-COOH) possesses oxygen-containing groups, including hydroxyl, carboxyl, and epoxy groups. That are present on both its basal plane and edges. These groups serve as reactive sites for covalent functionalization, as established in previous studies [18-24]. Various covalent functionalization techniques have been evaluated for GO & MWCNTs-COOH dispersion within a polymer matrix. [18].

Additionally, when combined in a nanocomposite, graphene oxide and carbon nanotube-oxidized conducting polymers, they create a synergistic effect, which enhances the insulating properties of the resulting material. The unique combination of these ingredients provides several benefits: (i) improved resistance of the nanocomposite against corrosion, (ii) improved thermal stability. Bars used in many applications are discussed, such as petrochemical plants, oil and gas wells, reinforcing bars in concrete, and the mining industry. Overall, the synergistic effect of combining graphene oxide, into a nanocomposite results in a material with good use as corrosion inhibitors, oil pipeline protection, heat resistance, conductivity, and other areas of interest, Relevance [33-41].

The aim of this investigation is to synthesize graphene oxide and oxidized carbon nanotubes independently, followed by the preparation of polyanthranilic acid and its combination with epoxy resin to form the mother liquor, with the final production of MWCNTs-COOH /Epoxy-PANA and GO- /Epoxy-PANA composites to study their effectiveness in inhibiting corrosion of low carbon steels in highly corrosive environments.

Finally, Anti-corrosion coatings are employed in various offshore platforms such as ships, offshore structures, steel bridges exposed to the seawater environment, and loads aboard oil tankers and bulk carriers. The reason for this is that corrosion can potentially degrade structural materials, facilitate fatigue cracks, brittle fracture, and unstable failure, which can then greatly impact the structural integrity of the entire structure. In light of this, our research utilized a polymeric nanocomposite as a corrosion inhibitor for low carbon steels, yielding favorable outcomes [42].

MATERIALS AND METHODS
Chemicals and Instrumentations

All the chemicals and solvents were acquired directly from the companies Sigma-Aldrich, SDH, or Riedel-de haën and were used in their original form without undergoing any purification or alteration. In order to analyze the materials prepared. Infrared spectroscopy was conducted using a Perkin Elmer FT-IR 65 instrument. X-ray diffraction analysis was performed using a Shimadzu XRD-6000 instrument with Cu Kα radiation (wavelength of 1.5406 Å). The surface of the samples was examined using a TESCAN MAIA3 scanning electron microscope. For TEM examination of the synthesized compounds, a Zeiss EM 10C-100 KV device from Germany, provided by Day-Petronic Co., was utilized. Lastly, the dielectric properties were investigated using a GW INSTEK LCR-8105G instrument with a frequency range spanning from 100 kHz to 5 MHz.

Synthesis of graphene oxide (GO) nanosheets

Graphene oxide was synthesized from graphite using a modified Hummer method. In a 250 ml reaction flask placed in an ice bath at 0°C, 0.50 g of graphite powder and 1.0 g of NaNO3 were combined with 23 ml of concentrated H2SO4 and stirred vigorously for 20 minutes. Subsequently, 3.0 g of KMnO4 was slowly added to the mixture with rapid stirring, while maintaining the temperature between 0-5°C. The mixture was then moderately stirred for one hour. Following this, 50.0 ml of water was cautiously added to the suspension under strong stirring. To dilute the prepared suspension, 150.0 ml of warm distilled water was added, and the concentration of remaining permanganate was reduced by dissolving manganese ions through the addition of 5.0 ml of hydrogen peroxide (30%). Finally, the resulting suspension was filtered, washed multiple times with warm distilled water, and subjected to ultrasonic treatment to exfoliate the GO into nanosheets. The nanosheets were subsequently dried in an oven at 90°C for 24 hours to obtain the GO powder. GO was synthesized using graphite as a starting material by the modified Hummer method [27,42].

Synthesis of Carbon nanotube oxidized (MWCNTs-COOH)

Carbon nanotube its oxidized by weight (1g) of carbon Nanotube by mixing it with two acids Sulfuric (H_2SO_4) and Nitric (HNO_3)in a ratio

of (4:1) (10 ml) of nitric acid with (40 ml) of sulfuric acid. It is stirred for (15 min), and the carbon Nanotube is gradually added to the mixture while maintaining the temperature between (60-70) °C. It is left to stir for (24 h), then the solution is taken and filtered by a centrifuge at a speed of (5000 RPM) for a period of (15 min, then the precipitate is washed and dried at a temperature of 80 °C. and examines its components [159-160].

Synthesis of poly (anthranilic acid) (PANA)

Poly anthranilic acid (2.05 g) was synthesized by polymerizing anthranilic acid with ammonium persulfate (APS) (6 g) in an aqueous solution of acetic acid at room temperature. Initially, 2.05 g of anthranilic acid was added to 50 ml of acetic acid (1 M) while stirring. The oxidizing agent APS, dissolved in 50 mL of distilled water, was then added drop by drop to the monomer solution. Once the addition was complete, the mixture was left to stir for 24 hours at room temperature. The resulting product was filtered, washed multiple times with 1 M acetic acid, and then rinsed with deionized water to remove any remaining acetic acid residue. The precipitate obtained was allowed to dry at room temperature for 48 hours [30,43].

Preparation of Epoxy-Poly (Anthranilic Acid) (PANA) Polymer composite (Mother Solution)

The mother solution, Epoxy-PANA, was prepared by directly mixing a poly (anthranilic acid) solution with epoxy resin. Firstly, 0.5 g of poly (anthranilic acid) (PANA) was dissolved in 30 ml of absolute ethanol and left stirring for 30 minutes until complete dissolution. Then, 30 ml of epoxy resin was gradually added to the polymeric solution while vigorously stirring until thorough mixing was achieved. The mixture was further stirred for one hour to ensure the formation of a homogeneous polymeric solution consisting of epoxy and poly (anthranilic acid) (Epoxy-PANA).

Preparation of Polymeric coating

Polymeric were coating prepared to examine their Corrosion rate and inhibition efficiency. The following procedure was followed for preparing the various polymeric coating described in Additionally, separate polymeric were coating prepared from nanostructures. A 0.05 gm of one of the nanostructure was added to a 10 ml of the mother solution (Epoxy- PANA), which was then suspended by ultrasound until a homogeneous

solution was obtained. Next, a 5 ml of hardener was added to the mixture, and it was further suspended by ultrasonic waves for 30 min. Finally, the resulting products were the polymeric coating, MWCNTs-CCOOH/Epoxy-PANA GO /Epoxy-PANA.

Measurement of Weight Loss

The corrosion rate values were determined by employing Eq. 1 utilizing the weight-loss approach. This non-electrochemical technique is extensively utilized to evaluate the corrosion rate and inhibitor efficiency, and it produces more dependable results than electrochemical procedures since it realistically accommodates experimental circumstances [44].

To ascertain the extent of weight loss endured by steel test samples that had been pre-cleaned and completely dried, said samples were initially weighed and then submerged into a beaker that contained 100 ml of 1 M HCl for a duration of 3 hours. The samples were subjected to both inhibited and uninhibited conditions, with the inhibitor GO/(PANA - Epoxy) and MWCNTs-COOH/(PANA - Epoxy) being tested for their corrosion rates and inhibition efficiency under varying temperatures in 1 M HCl. Meanwhile, the effects of different temperatures (namely 10, 20, 30, 40, and 50 degrees Celsius) on the aforementioned factors were also explored. The results were subsequently compiled into Tables 1 and 2. Corrosion rates (CR) in relation to low carbon steel were determined via weight reduction using the Eq. 1 [45].

$$C_R = \frac{\Delta W}{A \times t} \times 240000 \qquad (1)$$

Where: The weight loss (g) is represented by ΔW, while surface area (m^2) is denoted as A. The, and the time of exposure (day) is indicated as t. Where erosion rates are given in units of $/m^2$.day, which is denoted by (gmd) [124].

Where: To ascertain the inhibition efficiency (IE), the subsequent formula, which may be articulated in the form of Eq. 2, was employed [46].

$$IE\% = \frac{W_{uninh} - W_{inh}}{W_{uninh}} * 100 \qquad (2)$$

Including temperature and concentration, the experimental results were recorded in Table 3. It was observed that the corrosion rate increased with temperature but decreased with increasing inhibitor concentration. Furthermore, the inhibition efficiency increased with increasing

inhibitor concentration polymeric Nano composite and temperature.

RESULT AND DISCUSSION

FTIR

The FTIR spectrum of GO was presented in Fig. 1, revealing characteristic peaks at 3426, 1720, 1628, and 1058 cm-1, which can be assigned to v(O-H), v(C=O), v(C=C) in unoxidized graphite, and v(C-O), respectively [46]. As presented in Fig. 1, the FTIR spectrum of PANA exhibits distinct bands at 3370, 3210, 1690, 1607, 1517, and 1244 cm–1,

which can be attributed to v(O-H), v(N-H), v(C=O), v(C=C quinoid), v(C=C benzenoid), and v(C-H), respectively. It is noteworthy that these bands have been previously reported [30,47].

The FTIR spectra of MWCNTs-COOH (Prepared in an acidic medium) as shown in Fig. 2, where a broad and clear peak appears at (3428) cm-1, indicating the presence of carboxylic groups, and a bending frequency for (C-O) at (1397.5) cm-1 , and the presence of successive peaks at The frequency at (1672.5 cm−1) is associated with the stretching vibrations of carbonyl groups'(-C=O) ,

Table 1. Shows the impact of temperature on the corrosion rate of low carbon steels in 1M HCl without a corrosion inhibitor.

T (℃)	Corrosion Without inhibitor (g/ h . m)
10	102.7716
20	187.5916
30	732.2837
40	3444.6
50	7586.636

Table 2. Effect of temperature on the corrosion rate (CR) and inhibition efficiency (IE %) of corrosion of low carbon steels in 1M HCl in the presence of MWCNTs-COOH / (PANA-Epoxy) & GO/ (PANA-Epoxy) as acorrosion inhibitor.

T (°C)	MWCNTs-COOH /PANA-Epoxy (g/ h . m^2)	GO/ (PANA-Epoxy) (g/ h . m^2)
10	91.04957	73.44723
20	151.4897	125.5455
30	130.719	171.757
40	138.1499	146.1481
50	175.2714	178.1289

Table 3. Effect of temperature on the inhibition efficiency (IE %) of corrosion of low carbon steels in 1M HCl in the presence of MWCNTs-COOH / (PANA-Epoxy) & GO/ (PANA-Epoxy) as acorrosion inhibitor.

T (℃)	MWCNTs-COOH /PANA-Epoxy (IE%)	(PANA-Epoxy) / GO (IE%)
10	11.40592	28.53355
20	19.24494	33.07508
30	82.14914	76.54502
40	95.98938	95.75718
50	97.68973	97.65207

while the frequency (2914.5 cm-1) is evidence The presence of The vibrations of (C-H) stretching in alkyl groups, As for the out-of the level bending (in the fingerprint area) at a frequency of (774.5 cm-1), it indicates that there is no (O-H) interference at the tip, and the frequency at (1624.5 cm-1) corresponds to the double bond (C=C)'s bending vibration of deformation. and the absorption peaks found at (1049 cm-1) correspond to (C-O) group deformation vibrations. These (FTIR)

readings indicate that the reaction was successful [48].

XRD

In Fig. 3, the XRD spectra of graphite (Gt) and graphene oxide (GO) are presented. The XRD analysis of graphite (Fig. 3a) is crucial for discerning structural changes in the prepared graphitic materials. The XRD pattern of graphite reveals two distinct peaks at 2θ angles of 26.5°
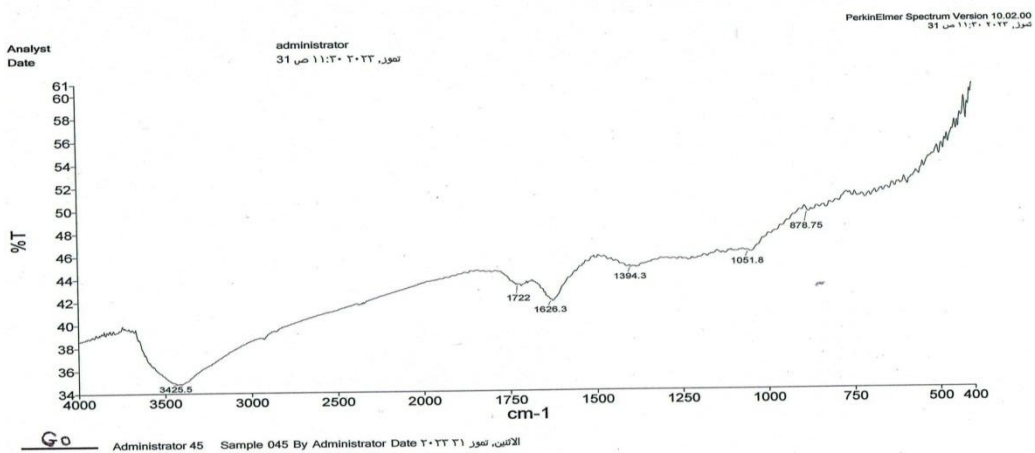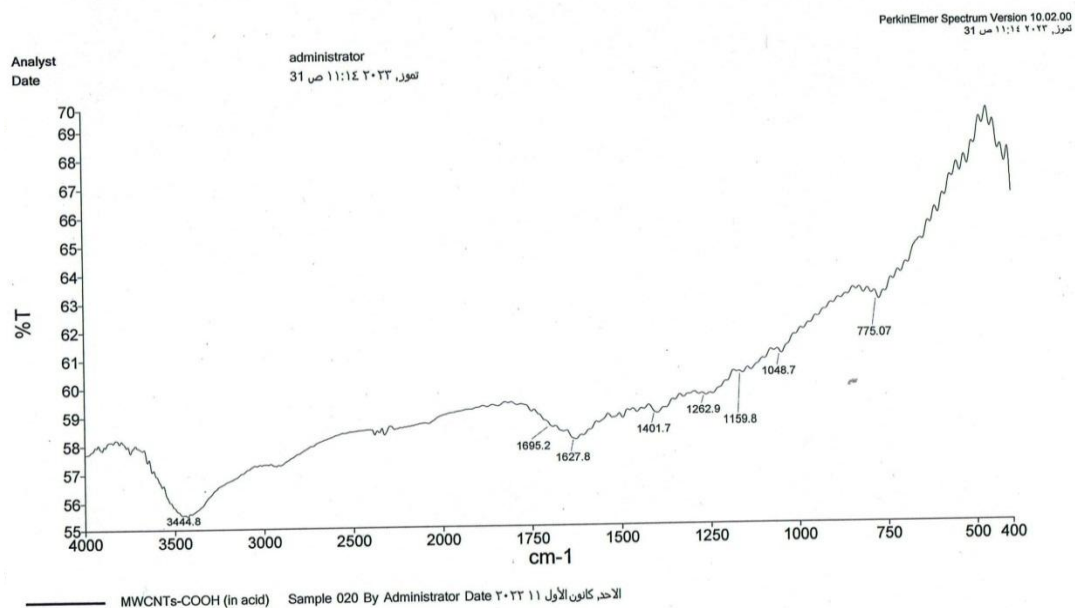

Fig. 1. FTIR of GO.

Fig. 2. FTIR of MWCNTs-COOH.

and 54.6°, corresponding to interlayer distances of 3.36 Å and 1.68 Å, respectively [49].

On the other hand, the XRD measurement of GO (Fig. 3b) exhibits a prominent peak at 2θ = 10.01°, indicating an interlayer distance of 8.75 Å. This peak is attributed to the presence of oxygen functional groups that form on the sheet surfaces during the oxidation process. Additionally, graphene oxide displays a peak at 2θ = 26.41°, resulting from partial exfoliation of the graphite [50]. Another peak observed at 2θ = 16.86° corresponds to graphite oxide, which is formed during the oxidation process [51,52].
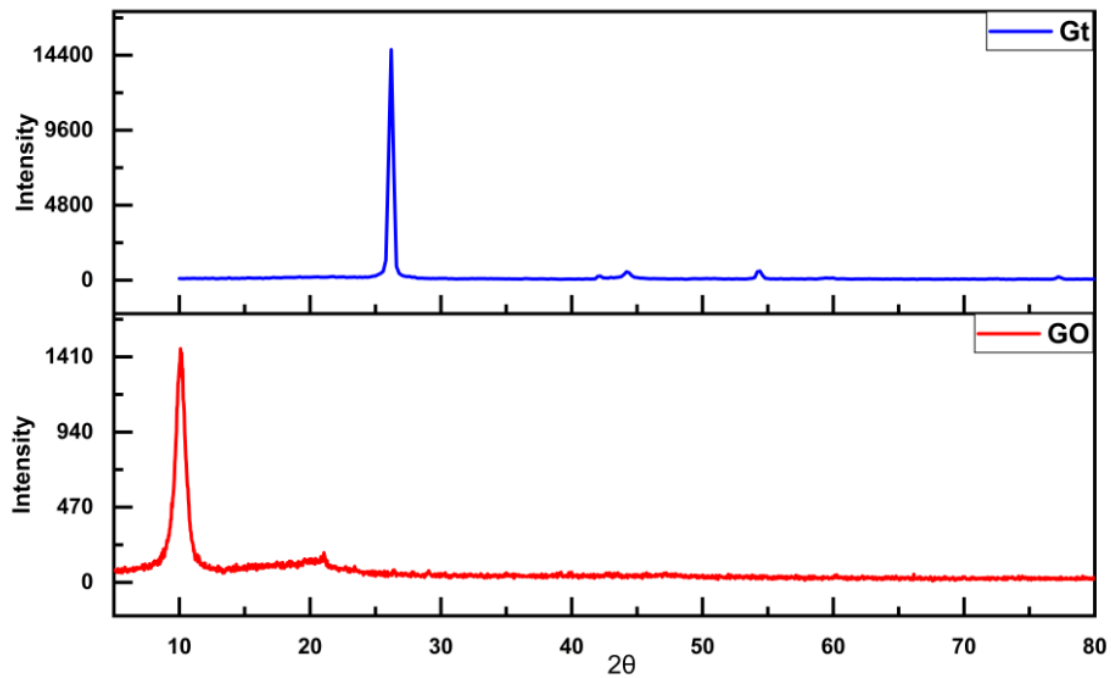
Fig. 4 displays the XRD spectrum of the
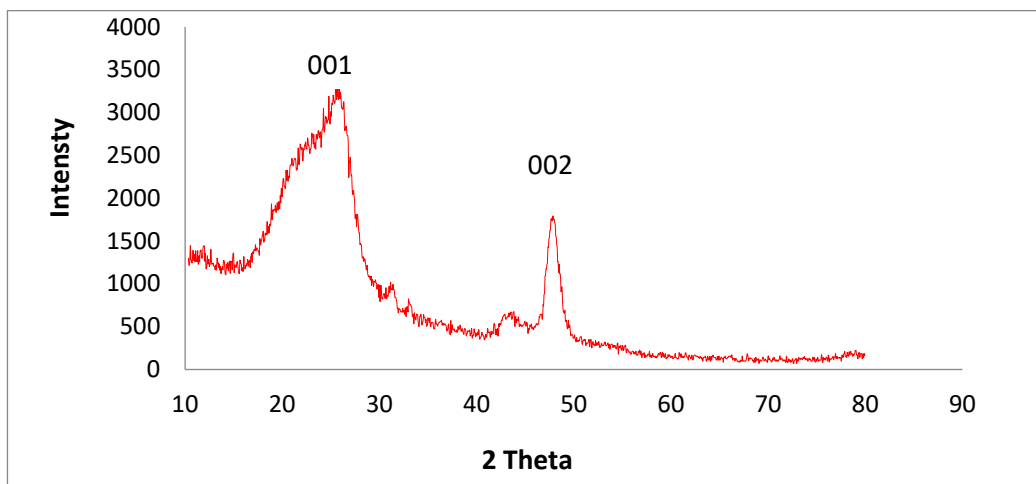

Fig. 3. XRD of graphite and graphene oxide.

Fig. 4. XRD of MWCNTs-COOH nanostructures.

synthesized MWCNTs-COOH nanoparticles. The diffractogram of MWCNTs-COOH nanoparticles exhibits distinct Cu Kα rays (λ = 1.5406Å) were utilized within the angle domain 2θ = 0.50°÷ 800° yen. Structural properties of MWCNTs-COOH were obtained by means of the hammer method using X-ray phase analysis, and the corresponding carbon peaks were observed in the spectrum. Two distinct peaks were observed in the spectrum, and the broadening of these peaks can be attributed to the presence of smaller particles. The X-ray diffraction peak of MWCNTs-COOH is distinctly discernible at (25.49 °). Consequently, the interlayer separation distance (d) is equivalent to (0.335898nm), and

this peak was characterized by the (001) index. Additionally, another peak is visible in the figure at (47.64°), representing the interlayer spacing ratio. This peak measures (0.192877nm), and it was identified by the (002) index. Fig. 4.

EDX

Fig. 5a-c displays the EDX spectra of Gt (graphite), GO (graphene oxide), and MWCNTs-COOH, respectively. The EDX analysis of graphite (Fig. 5a) indicates a 100% weight ratio of carbon signal at Kα = 0.27 keV [53-54]. On the other hand, the EDX analysis of GO (Fig. 5b) reveals a composition of GO nanosheets with a 52.21%
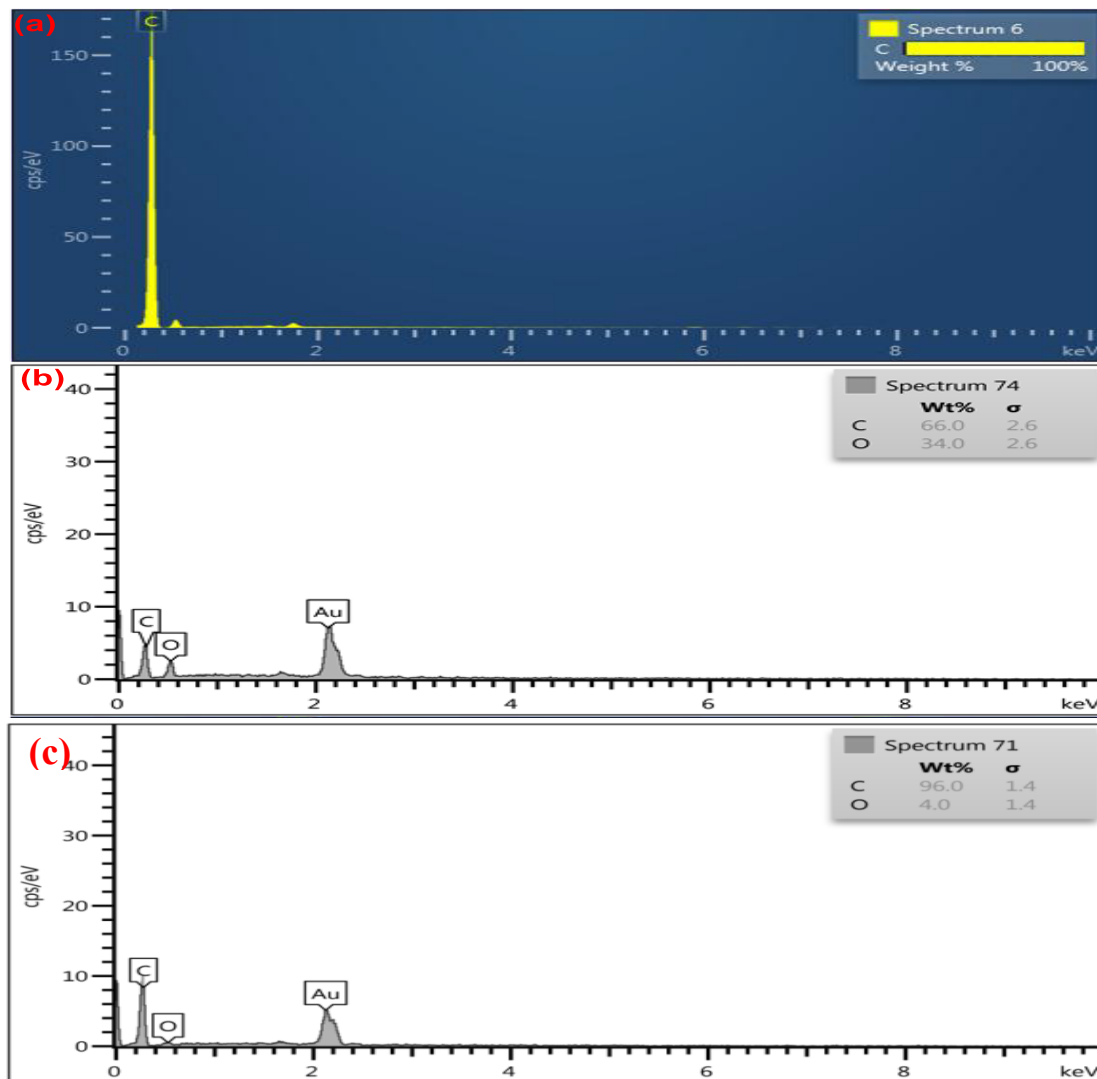

Fig. 5. EDX of (a) Gt, (b) GO, (c) MWCNTs.

weight ratio of carbon signal at Kα = 0.27 keV and a 47.79% weight ratio of oxygen signal at Kα = 0.50 keV. The higher oxygen content in graphene oxide compared to graphite is attributed to the oxidation processes involving strong oxidants such as $KMnO_4$, $NaNO_3$, and H_2SO_4 [55-60].

In the case of the spectra obtained through EDX analysis at spectrum 71 (as shown in (Fig. 5c) yield data comprising peaks that correspond to the diverse elements present in the sample. Each of these elements exhibits characteristic peaks with distinct energies, which have been extensively
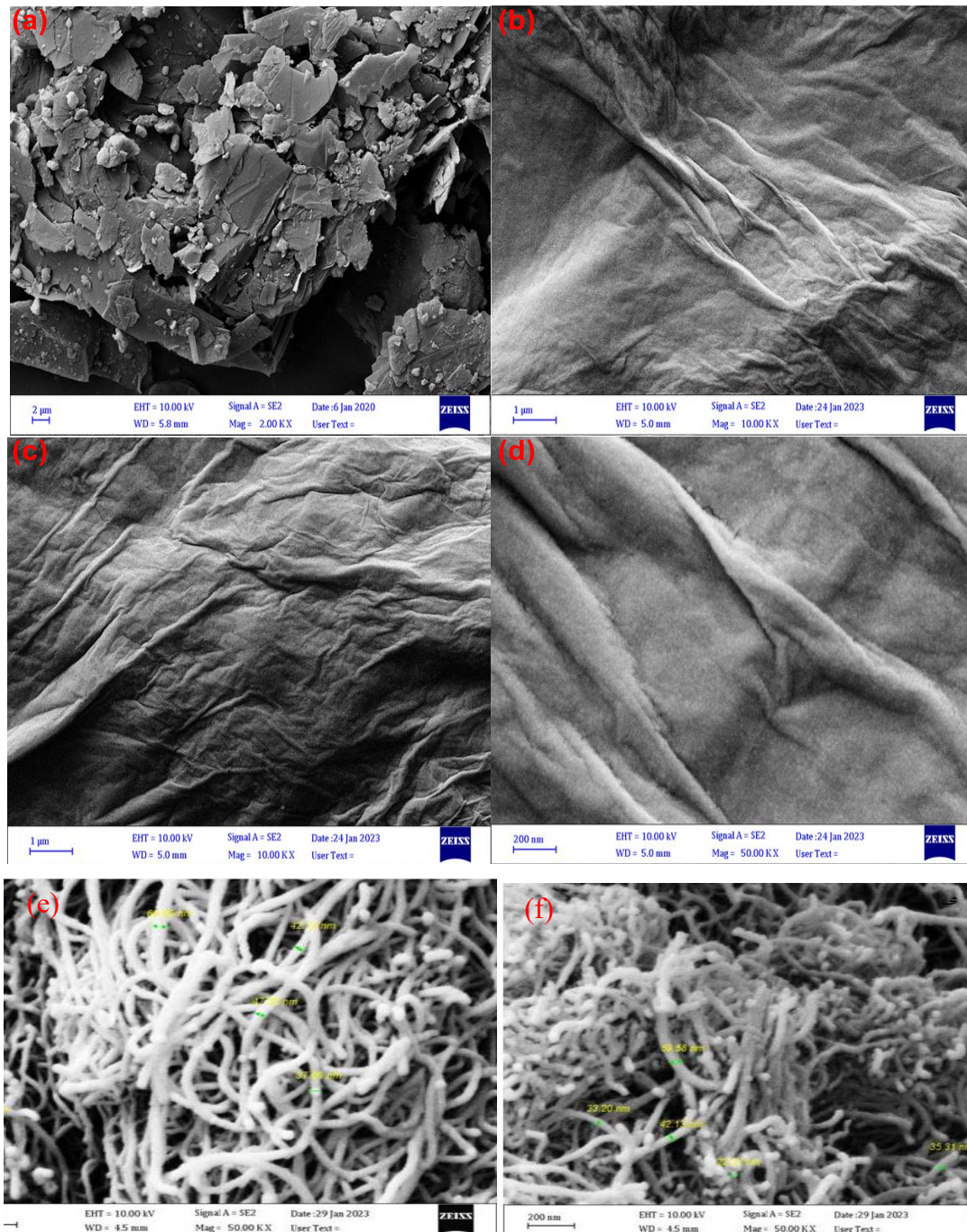

Fig. 6. FE-SEM of (a) Gt, (b-d) GO, (e, f) MWCNTs-COOH.

documented .The chemical composition of the compound under investigation is primarily carbon, comprising (96% of its mass), followed by oxygen, which constitutes(4% of its mass) . The presence of multi-walled carbon nanotubes functionalized with carboxylic acid (MWCNTs-COOH) has been successfully established through rigorous analysis. Additionally, our EDX analysis has revealed the

presence of gold (Au). This observation can be attributed to the fact that prior to conducting the elemental analysis, a scanning process was carried out . This is evidence of the presence of carboxyl groups -COOH.

FE-SEM

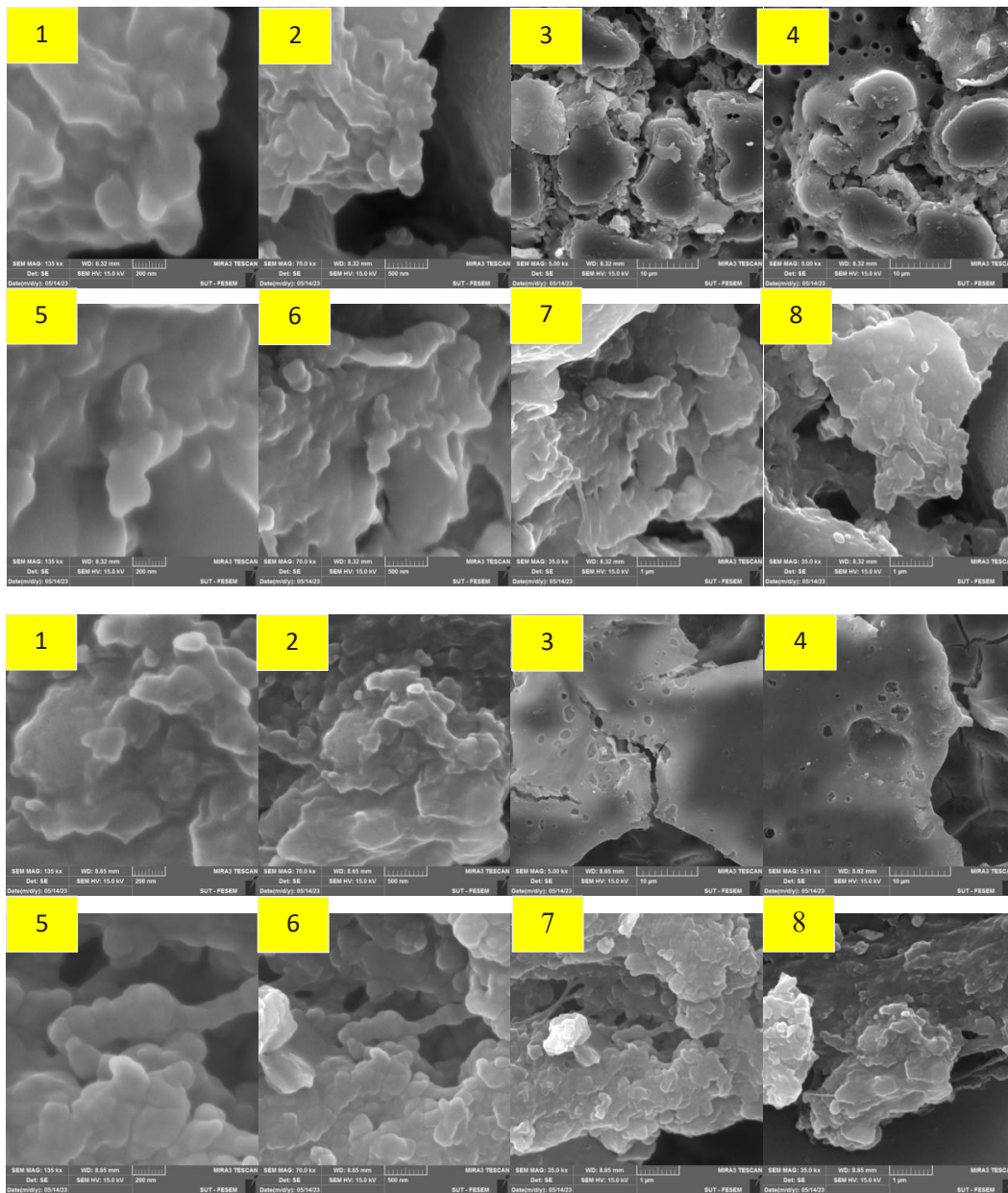The scanning electron microscope (FE-SEM)

Fig. 7.A(1-8)) Shown the study utilized Scanning Electron Microscopy (SEM) for corrosion of low carbon steel, after coating it with (MWCNTs-COOH/PANA-Epoxy), B(1-8)) Shown the study utilized Scanning Electron Microscopy (SEM) for corrosion of low carbon steel, after coating it with (GO/PANA-Epoxy).

is a sophisticated imaging tool extensively employed for examining the surface topography and dimensions of various samples at a nanoscale resolution. This technology finds widespread application in diverse scientific fields, including materials science, nanotechnology, biology, geology, and more, aiding in comprehensive

material analysis and research [61-66].

Fig. 6a-f shows the FE-SEM examination of graphite (Gt), graphene oxide (GO) nanosheets and nanoparticles (MWCNTs-COOH).The FE-SEM examination of the graphite shown in the figure (6.a) shows that it appears as a large block of graphite in the form of stacked sheets. Also, this
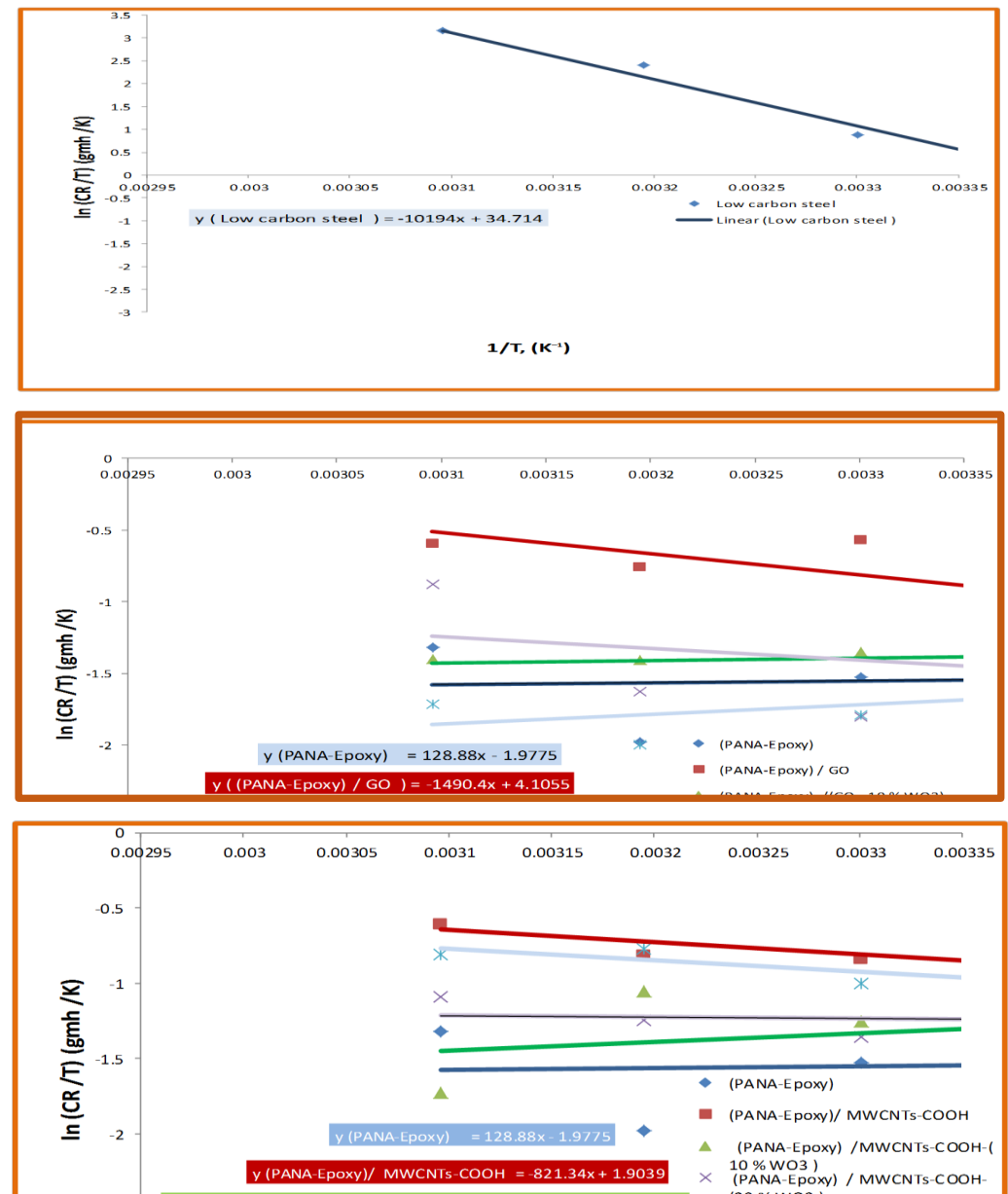

Fig. 8. A) Transition state diagram of corrosion of low carbon steel in (1M HCl), B) Transition state diagram of corrosion of low carbon steel in (1M HCl) in the presence of GO / PANA-Epoxy, C) Transition state diagram of corrosion of low carbon steel in (1M HCl) in the presence of MWCNTs-COOH / PANA-Epoxy.

large composition contains some deformations and small parts above the plates, and these results from the graphite grinding process.

Fig. 6.b-d presents the FE-SEM examination of graphene oxide nanosheets. It is noted from the figure that thin, smooth sheets appear that do not contain distortions and defects on the surface of the sheet, and this indicates the success of the used preparation method. It is also noted that there are some folds on the surface of the plate, and this is a result of the twisting of the plate itself or the accumulation of one part of the plate on another part of it, to be in this structure.

Figs. 6.e,f An FE-SEM scan of the MWCNTs-COOH nanoparticles is shown. The figure shows that the nanoparticles appear as filaments.It is also noted that there are some clusters of these particles, which leads to their appearance in the form of nanotubes.

Study (SEM) for corrosion of low carbon steel after coating with
GO /PANA-Epoxy, MWCNTs-COOH/PANA-Epoxy

The morphology of MWCNTs-COOH/PANA-Epoxy represents after immersion in (1M) HCL acid for (3 hours) and at (50 °C) in Fig. 7A (1-8). Due to the polymer's resistance to acid and its interaction with the acid and the formation of a protective layer that prevents corrosion of low-carbon steel. Figures show the non-dissolution of the polymer

and the strength of its bonding**.** It is noted from the figure that there is little corrosion despite the acid, temperature and time, and this is proven by the corrosion results in our current study, where the corrosion percentage was (175.2714) and the inhibition efficiency was (97.68973%).

The morphology of GO/ PANA-Epoxy for the nano composite after immersion in HCL (1M) acid for (3 hours) and at (50 °C). From the figure, we notice that the percentage of distortions on the surface of the alloy coated with this material is large compared to the case before adding tungsten oxide, due to the coating being affected by acid and heat, as the corrosion results showed that the corrosion rate is (178.1289) and the corrosion prevention efficiency is (97.65207%). Althoug in doing so, the coating thus prevents corrosion of low carbon steels. Figs. 7B (1-8)) show that, despite the acidity and high temperatures, the coating resisted corrosion [67-76].

Thermodynamic analysis

The transition state equation was used to evaluate the creation process of the polymeric nanocomposite.

$$\ln(C_R) = \ln A - \frac{E_a}{RT} \tag{3}$$

Whereas A, Ea, R, and T are defined as the frequency factor, activation energy, gas constant,

Table 4. Enthalpy and entropy of the corrosion process of low carbon steels with GO/PANA-Epoxy & MWCNTs-COOH/PANA-Epoxy in (1 M) of hydrochloric acid

Inhibitor	ΔS^*(J / mol . K)	ΔH^*(kJ / mol)
GO/ PANA-Epoxy	-163.4384556	12.3911856
MWCNTs-COOH/ PANA-Epoxy	-181.742558	6.82862076
Low carbon steel without inhibitor	-71.33180655	84.752916

Table 5. Corrosion activation energy values for low carbon steels in (1 M) of hydrochloric acid for GO/PANA-Epoxy & MWCNTs-COOH/PANA-Epoxy

Inhibitor	Ea (kJ / mol)
GO/ PANA-Epoxy	14.90201
MWCNTs-COOH/ PANA-Epoxy	9.339948
Low carbon steel without inhibitor	29.97197

and absolute temperature, respectively. The activation energy was determined by utilizing the Arrhenius plot of ln (CR) versus 1/T, wherein a slope of (-Ea/R) and an intercept of ln (A) were observed.

Where: Enthalpy activation (ΔH^*) and entropy (ΔS^*) were ascertained through the use of Figs. 8A and 8 B. The plotting of ln(CR/T) versus (1/T) facilitated the derivation of straight lines with slopes equivalent to (-ΔH^*/R) and intercepts equivalent to (ΔS^*/R)+ln(R/Nh). These values were subsequently tabulated in Tables 5 and 6. Notably, the dissolution process was found to be endothermic when positive enthalpies (ΔH^*) were observed [77]. According to literature, it has been suggested that a physisorption or chemisorption reaction would result in exothermicity, whereas a chemisorption reaction would lead to endothermicity [75-76].When the value of ΔS^* is negative, it may be attributed to the inhibitor molecules remaining unhydrolyzed in solution and instead forming a cross-linked network on the surface of low carbon steel. This, in turn, leads to a decrease in randomness as the reactants fail to move towards the low carbon steel. However, in graphene oxide, the addition of tungsten oxide in a certain percentage leads to the inhibitor tungsten oxide molecules becoming more regularly arranged on the surface of the sample. This eventually results in a decrease in entropy value as the percentage of tungsten oxide in graphene oxide increases. This observation is consistent with scientific experiments that have demonstrated the efficacy of increasing concentration [77-78]. Nevertheless, positive values of ΔS^* indicate a higher corrosion rate. [6,77-78].

In addition, the presence of GO/PANA-Epoxy and MWCNTs-COOH/PANA-Epoxy in (Table 6) causes the energy to decrease to (9.339948kJ/mol) in the case of MWCNTs-COOH/PANA-Epoxy. These data show that the activation energy (Ea) decreases, indicating a lower energy barrier for the inhibition reaction.A higher activation energy in the presence of this means that the activation energy decreases with increasing inhibition (corrosion inhibition).

CONCLUSION

Based on the results obtained from the analysis carried out, the following conclusions can be drawn:

1- It can be inferred that the rate of corrosion experienced by low carbon steel in a 1M HCl solution is directly proportional to the increase in temperature.

2- The coating prepared from the polymeric nanocomposite (PANA-Epoxy) with (graphene oxide) effectively inhibits the corrosion of low carbon steels in Corrosive solution $1M\ HCl$ and with different temperatures.

3- The coating prepared from the polymeric nanocomposite (PANA-Epoxy) with (carbon nano tube oxidized) effectively inhibits the corrosion of low carbon steels in Corrosive solution $1M\ HCl$ and with different temperatures.

4- The inhibition efficiency of the prepared coatings was observed to reach between 97.65207-97.68973)%. Increases with the difference of the nanocomposites and with the increase in temperature. On the other hand, the inhibition efficiency of the combined effect increases significantly when adding tungsten oxide, and also increases with the increase in temperature, effect ·It results from an increase in the percentage of the base component of the paint, which actually interacts with the surface of the paint and not the steel, because the paint protects the steel from corrosion.

4- The results from this study show a good agreement with the Linkmuir adsorption temperature. This is confirmed by the presented thermodynamic values, where negative standard free energy values indicate that the adsorption process is spontaneous and endothermic. Moreover, the entropy of the system undergoes a decrease during the process.

5-This particular study yields valuable insights into the inhibitory properties of polymeric nanocoatings under specific conditions. The use of polymeric nanocomposites is preferred due to their thermal hardening capabilities, which prevent decomposition at high temperatures and are thus more favorable than alternative inhibitor.

CONFLICT OF INTEREST

The authors declare that there is no conflict of interests regarding the publication of this manuscript.

REFERENCES

1. Song W, Zhao X, Jin Z, Fan L, Ji X, Deng J, et al. Poly(vinyl alcohol) for multi-functionalized corrosion protection of metals: A review. Journal of Cleaner Production. 2023;394:136390.
2. Ates B, Koytepe S, Ulu A, Gurses C, Thakur VK.

Chemistry, Structures, and Advanced Applications of Nanocomposites from Biorenewable Resources. Chem Rev. 2020;120(17):9304-9362.

3. Marcano DC, Kosynkin DV, Berlin JM, Sinitskii A, Sun Z, Slesarev A, et al. Improved Synthesis of Graphene Oxide. ACS Nano. 2010;4(8):4806-4814.

4. Joshi DJ, Koduru JR, Malek NI, Hussain CM, Kailasa SK. Surface modifications and analytical applications of graphene oxide: A review. TrAC, Trends Anal Chem. 2021;144:116448.

5. Kumar SSA, Bashir S, Ramesh K, Ramesh S. New perspectives on Graphene/Graphene oxide based polymer nanocomposites for corrosion applications: The relevance of the Graphene/Polymer barrier coatings. Prog Org Coat. 2021;154:106215.

6. Xavier JR. RETRACTED: Effect of surface modified WO$_3$ nanoparticle on the epoxy coatings for the adhesive and anticorrosion properties of mild steel. J Appl Polym Sci. 2019;137(5).

7. Kumar A, Ghosh PK, Yadav KL, Kumar K. Thermo-mechanical and anti-corrosive properties of MWCNT/epoxy nanocomposite fabricated by innovative dispersion technique. Composites Part B: Engineering. 2017;113:291-299.

8. Jin Y, Xia N, Gerhardt RA. Enhanced dielectric properties of polymer matrix composites with BaTiO3 and MWCNT hybrid fillers using simple phase separation. Nano Energy. 2016;30:407-416.

9. Montanheiro TLdA, Cristóvan FH, Machado JPB, Tada DB, Durán N, Lemes AP. Effect of MWCNT functionalization on thermal and electrical properties of PHBV/MWCNT nanocomposites. J Mater Res. 2014;30(1):55-65.

10. Ammar A, Al-Enizi AM, AlMaadeed MA, Karim A. Influence of graphene oxide on mechanical, morphological, barrier, and electrical properties of polymer membranes. Arabian Journal of Chemistry. 2016;9(2):274-286.

11. Khanam PN, Ponnamma D, Al-Madeed MA. Electrical Properties of Graphene Polymer Nanocomposites. Graphene-Based Polymer Nanocomposites in Electronics: Springer International Publishing; 2015. p. 25-47.

12. Wang Z, Nelson JK, Hillborg H, Zhao S, Schadler LS. Graphene Oxide Filled Nanocomposite with Novel Electrical and Dielectric Properties. Adv Mater. 2012;24(23):3134-3137.

13. Zuev VV, Shlikov AV. Polyamide 12/ fullerene C60 composites: investigation on their mechanical and dielectric properties. Journal of Polymer Research. 2012;19(8).

14. Dang B, Hu J, Zhou Y, He J. Remarkably improved electrical insulating performances of lightweight polypropylene nanocomposites with fullerene. J Phys D: Appl Phys. 2017;50(45):455303.

15. Wei W, Liu Z, Wei R, Han G-C, Liang C. Synthesis of MOFs/GO composite for corrosion resistance application on carbon steel. RSC advances. 2020;10(50):29923-29934.

16. Díez-Pascual AM, Luceño Sánchez JA, Peña Capilla R, García Díaz P. Recent Developments in Graphene/Polymer Nanocomposites for Application in Polymer Solar Cells. Polymers. 2018;10(2):217.

17. Chauhan DS, Quraishi MA, Ansari KR, Saleh TA. Graphene and graphene oxide as new class of materials for corrosion control and protection: Present status and future scenario. Prog Org Coat. 2020;147:105741.

18. Pourhashem S, Vaezi MR, Rashidi A, Bagherzadeh MR.

19. Wen N, Jiang B, Wang X, Shang Z, Jiang D, Zhang L, et al. Overview of Polyvinyl Alcohol Nanocomposite Hydrogels for Electro-Skin, Actuator, Supercapacitor and Fuel Cell. The Chemical Record. 2020;20(8):773-792.

20. Wu J, Cai C, Zhou Z, Qian H, Zha F, Guo J, et al. Low-cost mussel inspired poly(catechol/polyamine) coating with superior anti-corrosion capability on copper. Journal of Colloid and Interface Science. 2016;463:214-221.

21. Cao N, Miao Y, Zhang D, Boukherroub R, Lin X, Ju H, et al. Preparation of mussel-inspired perfluorinated polydopamine film on brass substrates: Superhydrophobic and anti-corrosion application. Prog Org Coat. 2018;125:109-118.

22. Phiri J, Johansson L-S, Gane P, Maloney T. A comparative study of mechanical, thermal and electrical properties of graphene-, graphene oxide- and reduced graphene oxide-doped microfibrillated cellulose nanocomposites. Composites Part B: Engineering. 2018;147:104-113.

23. Dagdag O, Berisha A, Mehmeti V, Haldhar R, Berdimurodov E, Hamed O, et al. Epoxy coating as effective anti-corrosive polymeric material for aluminum alloys: Formulation, electrochemical and computational approaches. J Mol Liq. 2022;346:117886.

24. Sahu G, Tripathy J, Sahoo BP. Significant enhancement of dielectric properties of graphene oxide filled polyvinyl alcohol nanocomposites: Effect of ionic liquid and temperature. Polym Compos. 2020;41(10):4411-4430.

25. Mohammed LA, Majeed AH, Hammoodi OG, Prakash C, Alheety MA, Buddhi D, et al. Design and characterization of novel ternary nanocomposite (rGO-MnO$_2$-PoPDA) product and screening its dielectric properties. International Journal on Interactive Design and Manufacturing (IJIDeM). 2022;17(5):2387-2401.

26. Majeed AH, Hussain DH, Al-Tikrity ETB, Alheety MA. Poly (o-Phenylenediamine-GO-TiO$_2$) nanocomposite: Modulation, characterization and thermodynamic calculations on its H2 storage capacity. Chemical Data Collections. 2020;28:100450.

27. Abd AN, Al-Agha AH, Alheety MA. Addition of Some Primary and Secondary Amines to Graphene Oxide, and Studying Their Effect on Increasing its Electrical Properties. Baghdad Science Journal. 2016;13(1):0097.

28. Maruthi N, Faisal M, Raghavendra N, Prasanna BP, Manohara SR, Revanasiddappa M. Anticorrosive polyaniline-coated copper oxide (PANI/CuO) nanocomposites with tunable electrical properties for broadband electromagnetic interference shielding. Colloids Surf Physicochem Eng Aspects. 2021;621:126611.

29. Kumar Mishra R, Goel S, Yazdani Nezhad H. Computational prediction of electrical and thermal properties of graphene and BaTiO$_3$ reinforced epoxy nanocomposites. Biomaterials and Polymers Horizon. 2021;1(1):1-14.

30. Majeed AH, Al-Tikrity ETB, Hussain DH. Dielectric properties of synthesized ternary hybrid nanocomposite embedded in poly (vinyl alcohol) matrix films. Polym Polym Compos. 2020;29(7):1089-1100.

31. Shirazi Z, Golikand AN, Keshavarz MH. A new nanocomposite based on poly (o-anthranilic acid), graphene oxide and functionalized carbon nanotube as an efficient corrosion inhibitor for stainless steel in severe environmental

corrosion. Composites Communications. 2020;22:100467.

32. Al-Hossainy AF, Bassyouni M, Zoromba MS. Elucidation of Electrical and Optical Parameters of Poly(o-anthranilic acid)-poly(o-amino phenol)/Copper Oxide Nanocomposites Thin Films. Journal of Inorganic and Organometallic Polymers and Materials. 2018;28(6):2572-2583.

33. Krishnan A, Joseph B, Bhaskar KM, Suma MS, Shibli SMA. Unfolding the anticorrosive characteristics of TiO_2– WO_3 mixed oxide reinforced polyaniline composite coated mild steel in alkaline environment. Polym Compos. 2018;40(6):2400-2409.

34. Su P-G, Peng S-L. Fabrication and NO2 gas-sensing properties of reduced graphene oxide/WO3 nanocomposite films. Talanta. 2015;132:398-405.

35. Rithin Kumar NB, Crasta V, Praveen BM. Dielectric and electric conductivity studies of PVA (Mowiol 10-98) doped with MWCNTs and WO_3 nanocomposites films. Materials Research Express. 2016;3(5):055012.

36. Li H, Zhang Y, Li C, Zhou Z, Nie X, Chen Y, et al. Cutting fluid corrosion inhibitors from inorganic to organic: Progress and applications. Korean J Chem Eng. 2022;39(5):1107-1134.

37. Palsaniya S, Nemade HB, Dasmahapatra AK. Graphene based PANI/MnO_2 nanocomposites with enhanced dielectric properties for high energy density materials. Carbon. 2019;150:179-190.

38. Ashery A, Maged FA. Novel Structure, Electric and Dielectric Properties of PPy-PANI-GO-MWCNTs Composite/MnO_2/Fe_3O_4/n-Si Structure. ECS Journal of Solid State Science and Technology. 2022;11(11):115004.

39. Han G, Liu Y, Zhang L, Kan E, Zhang S, Tang J, et al. MnO2 nanorods intercalating graphene oxide/polyaniline ternary composites for robust high-performance supercapacitors. Sci Rep. 2014;4:4824-4824.

40. Ji J, Zhang X, Huang Z, Yu X, Huang H, Huang Y, et al. One-Step Synthesis of Graphene Oxide/Polypyrrole/MnO₂ Ternary Nanocomposites with an Improved Electrochemical Capacitance. Journal of Nanoscience and Nanotechnology. 2017;17(6):4356-4361.

41. Soysal F, Çıplak Z, Getiren B, Gökalp C, Yıldız N. Synthesis and characterization of reduced graphene oxide-iron oxide-polyaniline ternary nanocomposite and determination of its photothermal properties. Mater Res Bull. 2020;124:110763.

42. Alheety NF, Majeed AH, Alheety MA. Silver Nanoparticles Anchored 5-methoxy benzimidazol thiomethanol (MBITM): Modulate, Characterization and Comparative Studies on MBITM and Ag-MBITM Antibacterial Activities. Journal of Physics: Conference Series. 2019;1294(5):052026.

43. Finšgar M, Jackson J. Application of corrosion inhibitors for steels in acidic media for the oil and gas industry: A review. Corros Sci. 2014;86:17-41.

44. Latif I, E. Al-Abodi E, H. Badri D, Al Khafagi J. Preparation, Characterization and Electrical Study of (Carboxymethylated Polyvinyl Alcohol/ZnO) Nanocomposites. American Journal of Polymer Science. 2013;2(6):135-140.

45. Ebrahimi R. The study of factors affecting the swelling of ultrasound-prepared hydrogel. Polym Bull. 2018;76(2):1023-1039.

46. Latif I, B. Alwan T, H. Al-Dujaili A. Low Frequency Dielectric Study of PAPA-PVA-GR Nanocomposites. Nanoscience and Nanotechnology. 2013;2(6):190-200.

47. Sophia IA, Gopu G, Vedhi C. Synthesis and Characterization of Poly Anthranilic Acid Metal Nanocomposites. Open Journal of Synthesis Theory and Applications. 2012;01(01):1-8.

48. Pang HF, Xiang X, Li ZJ, Fu YQ, Zu XT. Hydrothermal synthesis and optical properties of hexagonal tungsten oxide nanocrystals assisted by ammonium tartrate. physica status solidi (a). 2011;209(3):537-544.

49. Khan AA, Khan MQ, Iqbal M, Abid AY, Khan AR, Iqbal Y, et al. Facile synthesis of tungsten trioxide 3D architectures by a simple chemical solution route and photodegradation of Rhodamine B: structural, thermal, optical and impedance studies. Journal of Materials Science: Materials in Electronics. 2017;28(14):10357-10364.

50. Ain QT, Haq SH, Alshammari A, Al-Mutlaq MA, Anjum MN. The systemic effect of PEG-nGO-induced oxidative stress in vivo in a rodent model. Beilstein journal of nanotechnology. 2019;10:901-911.

51. Mishra AK, Ramaprabhu S. Carbon dioxide adsorption in graphene sheets. AIP Advances. 2011;1(3).

52. Zhang K, Zhang Y, Wang S. Enhancing thermoelectric properties of organic composites through hierarchical nanostructures. Sci Rep. 2013;3:3448-3448.

53. Boruah PJ, Khanikar RR, Bailung H. Synthesis and Characterization of Oxygen Vacancy Induced Narrow Bandgap Tungsten Oxide (WO_{3-x}) Nanoparticles by Plasma Discharge in Liquid and Its Photocatalytic Activity. Plasma Chem Plasma Process. 2020;40(4):1019-1036.

54. Liu F, Chen X, Xia Q, Tian L, Chen X. Ultrathin tungsten oxide nanowires: oleylamine assisted nonhydrolytic growth, oxygen vacancies and good photocatalytic properties. RSC Advances. 2015;5(94):77423-77428.

55. Use of Azadirachta indica (AZI) as green corrosion inhibitor against mild steel in acidic medium: anti-corrosive efficacy and adsorptive behaviour. International Journal of Corrosion and Scale Inhibition. 2017.

56. Zhang H, Yao M, Bai L, Xiang W, Jin H, Li J, et al. Synthesis of uniform octahedral tungsten trioxide by RF induction thermal plasma and its application in gas sensing. CrystEngComm. 2013;15(7):1432.

57. Kumar N, Sidhu GK, Kumar R. Correlation of synthesis parameters to the phase segregation and lattice strain in tungsten oxide nanoparticles. Materials Research Express. 2019;6(7):075019.

58. Al-Gaashani R, Najjar A, Zakaria Y, Mansour S, Atieh MA. XPS and structural studies of high quality graphene oxide and reduced graphene oxide prepared by different chemical oxidation methods. Ceram Int. 2019;45(11):14439-14448.

59. Kigozi M, Koech RK, Kingsley O, Ojeaga I, Tebandeke E, Kasozi GN, et al. Synthesis and characterization of graphene oxide from locally mined graphite flakes and its supercapacitor applications. Results in Materials. 2020;7:100113.

60. Aodah S, Bano N, Hussain I, AlSalhi MS. Quantitative analysis of the Schottky interface of reduced graphene oxide Schottky diodes. Materials Research Express. 2020;7(9):095007.

61. Hoseinzadeh S, Ghasemiasl R, Bahari A, Ramezani AH. The injection of Ag nanoparticles on surface of WO_3 thin film: enhanced electrochromic coloration efficiency and switching response. Journal of Materials Science: Materials in Electronics. 2017;28(19):14855-14863.

62. Nguyen DD, Dang DV, Nguyen DC. Hydrothermal synthesis and NH_3 gas sensing property of WO_3 nanorods at low temperature. Advances in Natural Sciences: Nanoscience and Nanotechnology. 2015;6(3):035006.

63. Kolhe PS, Shirke PS, Maiti N, More MA, Sonawane KM. Facile Hydrothermal Synthesis of WO3 Nanoconifer

Thin Film: Multifunctional Behavior for Gas Sensing and Field Emission Applications. Journal of Inorganic and Organometallic Polymers and Materials. 2018;29(1):41-48.

64. Alheety NF, Mohammed LA, Majeed AH, Aydin A, Ahmed KD, Alheety MA, et al. Antiproliferative and antimicrobial studies of novel organic-inorganic nanohybrids of ethyl 2-((5-methoxy-1H-benzo[d]imidazol-2-yl)thio)acetate (EMBIA) with TiO$_2$ and ZnO. J Mol Struct. 2023;1274:134489.

65. Adnan LA, Alheety NF, Majeed AH, Alheety MA, Akbaş H. Novel organic-inorganic nanohybrids (MnO2 and Ag nanoparticles functionalized 5-methoxy-2-mercaptobenzimidazole): One step synthesis and characterization. Materials Today: Proceedings. 2021;42:2700-2705.

66. Alheety MA, Majeed AH, Ali AH, Mohammed LA, Destagul A, Singh PK. Synthesis and characterization of eggshell membrane polymer-TiO2 nanocomposite for newly synthesized ionic liquid release. Journal of the Iranian Chemical Society. 2022;19(9):4005-4015.

67. Al-Tikrity ETB, Waheed IF, Ali SM. Study of electrical properties of a reduced graphene-oxadiazole-2-thiol (rGS) PVA polymer composite. Polym Polym Compos. 2018;27(1):11-19.

68. Jha SN, Narsaiah K, Basediya AL, Sharma R, Jaiswal P, Kumar R, et al. Measurement techniques and application of electrical properties for nondestructive quality evaluation of foods-a review. J Food Sci Technol. 2011;48(4):387-411.

69. Lim M, Kim D, Han H, Khan SB, Seo J. Water sorption and water-resistance properties of poly(vinyl alcohol)/clay nanocomposite films: Effects of chemical structure and morphology. Polym Compos. 2014;36(4):660-667.

70. Barber P, Balasubramanian S, Anguchamy Y, Gong S, Wibowo A, Gao H, et al. Polymer Composite and Nanocomposite Dielectric Materials for Pulse Power Energy Storage. Materials. 2009;2(4):1697-1733.

71. Wang Y, Wharton JA, Shenoi RA. Ultimate strength analysis of aged steel-plated structures exposed to marine corrosion damage: A review. Corros Sci. 2014;86:42-60.

72. Habeeb HA, Kadhum AAA. Kinetic Study of Photodegradation of Azo Dyes With TiO2 Under Visible Light. Journal of Al-Nahrain University Science. 2010;13(3):41-50.

73. de Souza FS, Spinelli A. Caffeic acid as a green corrosion inhibitor for mild steel. Corros Sci. 2009;51(3):642-649.

74. Aksh AK, Abdul Nabi AS. Red pepper extract as eco-friendly corrosion inhibitor for Carbon steel N80 in 1 M HCl: Electrochemical and surface morphological studies. Basrah Researches Sciences. 2024;50(1):20.

75. Afghanistan's economic prospects after Soviet occupation and Jihad (Islamic armed struggle), 1979-1993 : a thesis submitted in partial fulfillment of the requirements for the degree of master of science / by Abdul Haq Amiri: University of Arizona Libraries; 1989.

76. Zarrouk A, El Ouali I, Bouachrine M, Hammouti B, Ramli Y, Essassi EM, et al. Theoretical approach to the corrosion inhibition efficiency of some quinoxaline derivatives of steel in acid media using the DFT method. Res Chem Intermed. 2012;39(3):1125-1133.

77. Raghavendra N, Bhat JI. Chemical components of mature areca nut husk extract as a potential corrosion inhibitor for mild steel and copper in both acid and alkali media. Chem Eng Commun. 2017;205(2):145-160.

78. Chen XH, Chen CS, Xiao HN, Cheng FQ, Zhang G, Yi GJ. Corrosion behavior of carbon nanotubes–Ni composite coating. Surf Coat Technol. 2005;191(2-3):351-356.